Sains Malaysiana 48(10)(2019): 2285–2295
*http://dx.doi.org/10.17576/jsm-2019-4810-25*

# Stability Analysis of MHD Carreau Fluid Flow over a Permeable Shrinking Sheet with Thermal Radiation

(Analisis Kestabilan Aliran Bendalir MHD Carreau pada Permukaan Mengecut Boleh Telap dengan Terma Radiasi)

RUSYA IRYANTI YAHAYA*, NORIHAN MD ARIFIN & SITI SUZILLIANA PUTRI MOHAMED ISA

ABSTRACT

*Dual solutions are discovered in the problem of magnetohydrodynamics (MHD) boundary layer flow of Carreau fluid over a permeable shrinking sheet with thermal radiation. Therefore, a stability analysis is carried out to identify the stable solution of this problem. For the stability analysis, the problem is considered to be unsteady with time derivative introduced into the governing equations. Next, time-dependent solutions are substituted into these equations to form linear eigenvalue equations. The smallest eigenvalue of these equations is then computed using the* bvp4c *solver in MATLAB. The results showed that the first solution is stable, while the second solution is unstable. The first solution is physically meaningful and realizable in practice, and thus significant to the problem.*

*Keywords: Carreau fluid; MHD; shrinking sheet; stability analysis*

ABSTRAK

*Penyelesaian dual telah diperoleh dalam masalah aliran lapisan sempadan magnetohidrodinamik (MHD) bendalir Carreau terhadap permukaan telap mengecut dengan radiasi terma. Sehubungan dengan itu, analisis kestabilan dilakukan bagi mengenal pasti penyelesaian yang stabil dalam masalah ini. Bagi analisis kestabilan tersebut, masalah ini telah dipertimbangkan sebagai masalah yang tidak stabil dengan memperkenalkan terbitan masa ke dalam persamaan menakluk. Kemudian, penyelesaian bersandar masa digantikan ke dalam persamaan tersebut untuk menghasilkan persamaan nilai eigen linear. Nilai eigen terkecil bagi persamaan ini kemudiannya dihitung menggunakan solver* bvp4c *di MATLAB. Keputusannya menunjukkan bahawa penyelesaian pertama adalah stabil sementara penyelesaian kedua tidak stabil. Penyelesaian pertama adalah bermakna secara fizikal dan boleh direalisasikan dalam amalan sebenar. Oleh itu, penyelesaian pertama adalah penting bagi masalah ini.*

*Kata kunci: Analisis kestabilan; bendalir Carreau; MHD; permukaan mengecut*

## INTRODUCTION

Carreau fluid is a generalized Newtonian fluid introduced by Pierre J. Carreau in 1968 (Irgens 2014). At a low shear rate, Carreau fluid has the behaviour of a Newtonian fluid, while at a high shear rate, the fluid behaves as a power-law fluid. The examples of Carreau fluid are polymeric solutions, such as 1% methylcellulose tylose in glycerol solution and 0.3% hydroxyethyl-cellulose Natrosol HHX in glycerol solution (Khan et al. 2016).

There are several studies on Carreau fluid flow over shrinking surfaces. This flow usually occurs in the process of rubber and plastic sheets production, hot rolling, and cooling of metallic plates (Bhatti et al. 2016). In most metallurgical and metal-working processes, magnetohydrodynamics (MHD) flow and heat transfer are considered. The presence of a magnetic field in the flow of electrically conducting fluid has great importance in controlling the boundary layer flow and the performance of many systems, such as, in a nuclear reactor and MHD generator (Soid et al. 2018). Besides that, the MHD flow has broad applications in engineering and medical engineering fields, as studied by Alamri et al. (2019), Bhatti et al. (2018), Sheikholeslami et al. (2019), and Sohail et al. (2019). Meanwhile, the first study on MHD flow of non-Newtonian fluid was done by Sarpkaya (1961). Later, Akbar et al. (2014) studied the MHD stagnation-point flow of Carreau fluid over a permeable linearly shrinking sheet. Dual solutions were obtained in this study. Suneetha and Gangadhar (2015) extended the study with the effects of thermal radiation and convective boundary condition. Then, Naganthran and Nazar (2016) performed stability analysis to the dual solutions obtained in MHD stagnation-point flow of Carreau fluid over a shrinking sheet. The effects of nonlinear thermal radiation to the MHD stagnation-point flow was studied by Hashim et al. (2017), while Arifin et al. (2017) discussed the slip effects. Next, Hashim and Khan (2017) studied the MHD flow over a shrinking cylinder with chemical species diffusion. Recently, Santhosh et al. (2019, 2018) studied the MHD flow of Carreau fluid over a shrinking surface in the suspension of dust and nanoparticles. In these studies, heat generation is considered.

Since the vorticity flow over a shrinking surface is not confined within a boundary layer, suction or stagnation

flow is added to obtain the solutions for flow over shrinking surfaces (Lok et al. 2011). The study of fluid flow over shrinking surfaces, especially with suction, usually results in dual solutions; this includes the studies on Carreau fluid flow (Khan et al. 2018; Miklavčič & Wang 2006). The significance and stability of the solutions can be determined through stability analysis. This analysis was first carried out by Merkin (1986) to the dual solutions obtained in mixed convection flow. In this study, the stable solution was found to be the first solution, while the second solution was unstable. The recent studies on stability analysis of solutions were by Hashim et al. (2018a) and Kamal et al. (2019).

In the present paper, the MHD flow of Carreau fluid over a nonlinear shrinking sheet with thermal radiation is studied, which extends the problem by Khan et al. (2016) to the case of shrinking sheet and stability analysis. Based on previous studies, the results are expected to be of dual solutions. Therefore, a stability analysis will be carried out, and the results will be discussed.

## MATHEMATICAL FORMULATION

### STEADY PROBLEM

Consider a steady, incompressible, two-dimensional boundary layer flow of Carreau fluid over a sheet that shrinks with a nonlinear velocity of $u = U_w(x)$. For a nonlinearly shrinking sheet, we consider a general power-law surface velocity, $U_w(x) = ax^m$ where $a < 0$ for shrinking and $m$ is positive ($m > 0$). However, the value of $m = 1$ is not considered in this study as it corresponds to the linear velocity of the sheet, $U_w(x) = ax$. As illustrated in Figure 1, the shrinking sheet is located along the x-axis while the y-axis normal to it. Meanwhile, the Carreau fluid is considered to flow in the region $y \geq 0$ with a magnetic field of strength $B_0$ applied in the direction perpendicular to the sheet. The effect of thermal radiation is considered in this problem, while the induced magnetic field is omitted due to the assumption of very small magnetic Reynolds number.

The governing equations of the problem are as follows (Khan et al. 2016):

$$\frac{\partial u}{\partial x}+\frac{\partial v}{\partial y}=0, \tag{1}$$

$$\frac{\partial u}{\partial x}+v\frac{\partial u}{\partial y}=v\frac{\partial^2 u}{\partial y^2}\left[1+\Gamma^2\left(\frac{\partial u}{\partial y}\right)^2\right]^{\frac{n-1}{2}}+$$

$$v(n-1)\Gamma^2\frac{\partial^2 u}{\partial y^2}\left(\frac{\partial u}{\partial y}\right)^2\left[1+\Gamma^2\left(\frac{\partial u}{\partial y}\right)^2\right]^{\frac{n-3}{2}}$$

$$-\frac{\sigma B_0^2}{\rho}u, \tag{2}$$

$$u\frac{\partial T}{\partial x}+v\frac{\partial T}{\partial y}=\alpha\frac{\partial^2 T}{\partial y^2}-\frac{1}{\rho c_p}\frac{\partial q_r}{\partial y}, \tag{3}$$

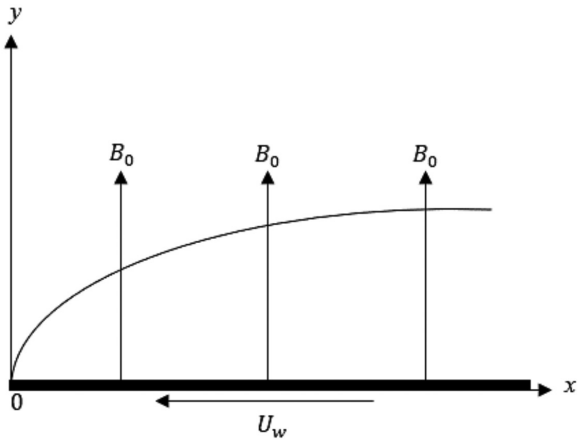


FIGURE 1. Schematic diagram of the problem

with the boundary conditions:

$$u = U_w(x) = ax^m, \qquad v = v_w,$$

$$-k\frac{\partial T}{\partial y} = h_f(T_f - T) \qquad \text{at } y = 0, \tag{4}$$

$$u \to 0, \qquad T \to T_\infty \qquad \text{as } y \to \infty, \tag{5}$$

where $u$ and $v$ are the velocity components along the $x$- and $y$-axes, $\rho$ respectively, is the fluid density, $\nu = \frac{\mu}{\rho}$ is the kinematic viscosity of the fluid with $\mu$ as the dynamic viscosity, $\Gamma$ is the material constant called relaxation time, $\sigma$ is the electrical conductivity of the fluid, $T$ is the fluid temperature, $q_r$ is the radiative heat flux, $\alpha = \frac{k}{\rho c_p}$ is the thermal diffusivity with $k$ as the thermal conductivity and $c_p$ is the specific heat, $v_w$ is the mass transfer velocity, $h_f$ is the convective heat transfer coeffcient, $T_f$ is the convective fluid temperature below the moving sheet and $T_\infty$ is the ambient fluid temperature.

In the equations, $n$ is the power-law index used to determine fluid behaviour where the value of $0 < n < 1$ indicates the fluid as a pseudoplastic fluid, $n > 1$ indicates the fluid as a dilatant fluid and $n = 1$ describes the fluid as a Newtonian fluid.

Since the flow is considered over a heated horizontal flat plate, the radiative heat flux expression in (3) can be simplified by using the Rosseland approximation (Khan et al. 2016),

$$q_r = -\frac{16\sigma^*}{3k^*}T^3\frac{\partial T}{\partial y}, \tag{6}$$

where $\sigma^*$ is the Stefan-Boltzmann constant and $k^*$ is the mean absorption coeffcient. Substitute (6) into (3) to obtain:

$$u\frac{\partial T}{\partial x}+v\frac{\partial T}{\partial y}=\frac{\partial}{\partial y}\left[\left(a+\frac{16\sigma^* T^3}{3k^*\rho c_p}\right)\frac{\partial T}{\partial y}\right]. \tag{7}$$

Then, the following transformations are used to reduce (1), (2) and (7) to nonlinear ordinary differential equations (Khan et al. 2016):

$$\psi = \sqrt{\frac{2\nu b}{m+1}} x^{\frac{m+1}{2}} f(\eta), \quad \eta = y\sqrt{\frac{b(m+1)}{2\nu}} x^{\frac{m+1}{2}},$$

$$\theta(\eta) = \frac{T - T_\infty}{T_f - T_\infty}, \tag{8}$$

with $\eta$ as the similarity variable; $b$ as the constant and $\psi$ as the stream function. The resulting nonlinear ordinary differential equations are:

$$\left[1 + nWe^2\left(f''\right)^2\right]\left[1 + We^2\left(f''\right)^2\right]^{\frac{n-3}{2}} f''' +$$

$$ff'' - \left(\frac{2m}{m+1}\right)\left(f'\right)^2 - M^2 f' = 0, \tag{9}$$

$$\theta'' + Prf\theta' + \frac{4}{3N_R}\frac{d}{d_\eta}\left[\left(1 + \left(\theta_w - 1\right)\theta\right)^{3\theta'}\right] = 0, \tag{10}$$

with boundary conditions:

$$f(0) = s,\ f'(0) = \lambda\ \ \theta'(0) = -\phi\,[1 - \theta(0)], \tag{11}$$

$$f'(\infty) \to 0,\ \theta(\infty) \to 0, \tag{12}$$

where the prime represents ordinary derivative with respect to $\eta$. In the above equations, $We^2 = \frac{b^3(m+1)\Gamma^2 x^{3m-1}}{2\nu}$ is the local Weissenberg number, $M^2 = \frac{2\sigma B_0^2}{\rho b(m+1)x^{m-1}}$ is the magnetic parameter, $Pr = \frac{\mu c_p}{k}$ is the Prandtl number, $N_R = \frac{kk^*}{4\sigma^* T_\infty^3}$ is the non-linear radiation parameter, $\phi = \frac{h_f}{k}\sqrt{\frac{2\nu}{b(m+1)}} x^{\frac{1-m}{2}}$ is the local Biot number, $\theta_w = \frac{T_f}{T_\infty}$ is the temperature ratio parameter with $\theta_w > 1$, $\lambda = \frac{a}{b}$ is the shrinking parameter with $\lambda < 0$ for shrinking sheet and $s = -v_w\left(\sqrt{\frac{2}{\nu b(m+1)}} x^{\frac{1-m}{2}}\right)$ is the mass transfer parameter with $s > 0$ for suction.

Equations (9) and (10) are solved subject to the boundary conditions (11) and (12) using the *bvp4c* solver in MATLAB.

Following Khan et al. (2016), the physical quantities of interest are the local skin friction coeffcient and the local Nusselt number, which are given by:

$$C_{fx} = \frac{\tau_w}{\rho(U_w(x))^2}, \quad Nu_x = \frac{xq_w}{k(T_f - T_\infty)}, \tag{13}$$

respectively. The wall shear stress, $\tau_w$ and wall heat transfer, $q_w$ are given by:

$$\tau_w = \mu\frac{\partial u}{\partial y}\left[1 + \Gamma^2\left(\frac{\partial u}{\partial y}\right)^2\right]^{\frac{n-1}{2}}\Bigg|_{y=0}, \quad q_w = -k\left(\frac{\partial T}{\partial y}\right) + q_r\Big|_{y=0}. \tag{14}$$

By substituting (14) into (13), we obtain:

$$Re^{1/2} Cf_x = \frac{1}{\lambda^2}\sqrt{\frac{m+1}{2}} f''(0), \tag{15}$$

and

$$Re^{-1/2} Nu_x = -\sqrt{\frac{m+1}{2}}\theta'(0)\left[1 + \frac{4}{3N_R}\right]. \tag{16}$$

In the equations, $Re = \frac{bx^{m+1}}{\nu}$ is the local Reynolds number.

## STABILITY ANALYSIS

Now, the problem is considered to be unsteady. The continuity (1) holds and time derivative is introduced into (2) and (3) to obtain:

$$\frac{\partial u}{\partial t} + u\frac{\partial u}{\partial x} + v\frac{\partial u}{\partial y} = \nu\frac{\partial^2 u}{\partial y^2}\left[1 + \Gamma^2\left(\frac{\partial u}{\partial y}\right)^2\right]^{\frac{n-1}{2}}$$

$$+ \nu(n-1)\Gamma^2\frac{\partial^2 u}{\partial y^2}\left(\frac{\partial u}{\partial y}\right)^2 \tag{17}$$

$$\frac{\partial T}{\partial t} + u\frac{\partial T}{\partial x} + v\frac{\partial T}{\partial y} = \alpha\frac{\partial^2 T}{\partial y^2} - \frac{1}{\rho c_p}\frac{\partial q_\tau}{\partial y}, \tag{18}$$

where $t$ is for time.

Then, the following similarity transformations are introduced:

$$\psi = \sqrt{\frac{2\nu b}{m+1}} x^{\frac{m+1}{2}} f(\eta,\tau), \quad \eta = y\sqrt{\frac{b(m+1)}{2\nu}} x^{\frac{m-1}{2}},$$

$$\theta(\eta,\tau) = \frac{T - T_\infty}{T_f - T_\infty}, \tag{19}$$

with $\tau = btx^{m-1}$ as the dimensionless time variable (Mahapatra & Nandy 2011).

The similarity transformations (19) is substituted into (17) and (18) to obtain:

$$\left[1 + nWe^2\left(\frac{\partial^2 f}{\partial\eta^2}\right)^2\right]\left[1 + We^2\left(\frac{\partial^2 f}{\partial\eta^2}\right)^2\right]^{\frac{n-3}{2}}$$

$$\frac{\partial^3 f}{\partial\eta^3} + f\frac{\partial^2 f}{\partial\eta^2} - \left(\frac{2m}{m+1}\right)\left(\frac{\partial f}{\partial\eta}\right)^2 - M^2\frac{\partial f}{\partial\eta}$$

$$-2\tau\left(\frac{m-1}{m\neq 1}\right)\left(\frac{\partial f}{\partial\eta}\frac{\partial^2 f}{\partial\eta\partial\tau} + \frac{\partial f}{\partial\tau}\frac{\partial^2 f}{\partial\eta^2}\right) - \left(\frac{2}{m+1}\right)\frac{\partial^2 f}{\partial\eta\partial\tau} = 0, \tag{20}$$

$$\frac{\partial^2\theta}{\partial\eta^2}+Prf\frac{\partial\theta}{\partial\eta}+\frac{4}{3N_R}\frac{\partial}{\partial\eta}\left[(1+(\theta_w-1)\theta)^3\frac{\partial\theta}{\partial\eta}\right]$$

$$-2Prr\left(\frac{m-1}{m+1}\right)\left(\frac{\partial\theta}{\partial\tau}\frac{\partial f}{\partial\eta}-\frac{\partial f}{\partial\tau}\frac{\partial\theta}{\partial\eta}\right)-Pr\left(\frac{2}{m+1}\right)\frac{\partial\theta}{\partial\tau}=0. \quad (21)$$

with the boundary conditions:

$$f(0,\tau)=s, \qquad \frac{\partial}{\partial\eta}f(0,\tau)=\lambda,$$

$$\frac{\partial}{\partial\eta}\theta(0,\tau)=-\phi[1-\theta(0,\tau)], \quad (22)$$

$$\frac{\partial}{\partial\eta}f(\infty,\tau)\to 0, \qquad \theta(\infty,\tau)\to 0. \quad (23)$$

Following Hashim et al. (2018a, 2018b), we let n = 3 to obtain:

$$\left[1+3We^2\left(\frac{\partial^2 f}{\partial\eta^2}\right)^2\right]\frac{\partial^3 f}{\partial\eta^3}+f\frac{\partial^2 f}{\partial\eta^2}-\left(\frac{2m}{m+1}\right)\left(\frac{\partial f}{\partial\eta}\right)^2-M^2\frac{\partial f}{\partial\eta}-$$

$$2\tau\left(\frac{m-1}{m+1}\right)\left(\frac{\partial f}{\partial\eta}\frac{\partial^2 f}{\partial\eta\partial\tau}+\frac{\partial f}{\partial\tau}\frac{\partial^2 f}{\partial\eta^2}\right)-\left(\frac{2}{m+1}\right)\frac{\partial^2 f}{\partial\eta\partial\tau}=0. \quad (24)$$

The stability of the steady flow solutions, and for the boundary value problem (9)-(12) can be identified by introducing the following form of solutions (Weidman et al. 2006):

$$f(\eta,\tau)=f_0(\eta)+e^{-\gamma\tau}F(\eta,\tau),$$

$$\theta(\eta,\tau)=\theta_0(\eta)+e^{-\gamma\tau}G(\eta,\tau), \quad (25)$$

where $F(\eta,\tau)$ and $G(\eta,\tau)$ are small relative to $f_0(\eta)$ and $\theta_0(\eta)$ while $\gamma$ is the unknown eigenvalue. Equation (25) is substituted into (21)-(24) to obtain:

$$\left[1+3We^2\left(\frac{\partial^2 f_0}{\partial\eta^2}\right)^2\right]\frac{\partial^3 F}{\partial\eta^3}+\left[f_0+6We^2\frac{\partial^2 f_0}{\partial\eta^2}\frac{\partial^3 f_0}{\partial\eta^3}\right]\frac{\partial^2 F}{\partial\eta^2}$$

$$+\left[\left(\frac{2}{m+1}\right)\left(\gamma-2m\frac{\partial f_0}{\partial\eta}\right)-M^2\right]\frac{\partial F}{\partial\eta}+F\frac{\partial^2 f_0}{\partial\eta^2}-2\tau\left(\frac{m-1}{m+1}\right)$$

$$\left(-\gamma\frac{\partial f_0}{\partial\eta}\frac{\partial F}{\partial\eta}+\frac{\partial f_0}{\partial\eta}\frac{\partial^2 F}{\partial\eta\partial\tau}-\gamma F\frac{\partial^2 f_0}{\partial\eta^2}+\frac{\partial F}{\partial\tau}\frac{\partial^2 f_0}{\partial\eta^2}\right)$$

$$-\left(\frac{2}{m+1}\right)\frac{\partial^2 F}{\partial\eta\partial\tau}=0, \quad (26)$$

$$\left(1+\frac{4}{3N_R}(1+(\theta_w-1)\theta_0)^3\right)\frac{\partial^2 G}{\partial\eta^2}+Prf_0\frac{\partial G}{\partial\eta}\left(\frac{2}{m+1}\right)\gamma G+PrF\frac{\partial\theta_0}{\partial\eta}$$

$$+\frac{4}{N_R}\left[(\theta_w-1)(1+(\theta_w-1)\theta_0)\left(2(\theta_w-1)G\left(\frac{\partial\theta_0}{\partial\eta}\right)^2\right.\right.$$

$$\left.\left.+2(1+(\theta_w-1)\theta_0)\frac{\partial\theta_0}{\partial\eta}\frac{\partial G}{\partial\eta}+(1+(\theta_0)G\frac{\partial^2\theta_0}{\partial\eta^2}\right)\right]$$

$$-2Pr\tau\left(\frac{m-1}{m+1}\right)\left(-\gamma G\frac{\partial f_0}{\partial\eta}+\frac{\partial G}{\partial\tau}\frac{\partial f_0}{\partial\eta}+\gamma F\frac{\partial\theta_0}{\partial\eta}-\frac{\partial F}{\partial\eta}\frac{\partial\theta_0}{\partial\eta}\right)$$

$$-Pr\left(\frac{2}{m+1}\right)\frac{\partial G}{\partial\tau}=0, \quad (27)$$

$$F(0,\tau)=0\ \frac{\partial}{\partial\eta}F(0,\tau)=0,\ \frac{\partial}{\partial\eta}G(0,\tau)=\phi G(0,\tau) \quad (28)$$

$$\frac{\partial}{\partial\eta}F(\infty,\tau)\to 0,\ G(\infty,\tau)\to 0. \quad (29)$$

According to Weidman et al. (2006), the value of $\tau$ is set to zero so that the initial decay or growth of disturbance in (25) can be identified. Thus, $F = F_0(\eta)$ and $G = G_0(\eta)$, then (26)-(29) become:

$$[1+3We^2(f'')^2F_0''']+(f_0+6We^2f_0''f_0''']F_0''$$

$$+\left[\left(\frac{2}{m+1}\right)(\gamma-2mf_0')-M^2\right]F_0'+F_0f_0''=0, \quad (30)$$

$$\left[1+\frac{4}{3N_R}(1+(\theta_w-1)\theta_0)^3\right]G_0''+Prf_0G_0'+Pr\left(\frac{2}{m+1}\right)\gamma G_0+PrF_{0\theta_0'}$$

$$+\frac{4}{N_R}[(\theta_w-1)(1+(\theta_w-1)\theta_0)(2(\theta_w-1)G_0(\theta_0')^2$$

$$+2(1+(\theta_w-1)\theta_0)\theta_0'G_0'+(1+(\theta_w-1)G_0\theta_0'')]=0, \quad (31)$$

$$F_0(0)=0,\ F_0'(0)=0,\ G_0'=\phi G_0(0), \quad (32)$$

$$F_0'(\infty)\to 0,\ G_0(\infty)\to 0. \quad (33)$$

These equations will produce an infinite set of eigenvalues ($\gamma_1<\gamma_2<\gamma_3<\ldots$) (Awaludin et al. 2016). If $\gamma_1>0$, the flow is stable due to an initial decay of disturbance. Meanwhile, the opposite occurs when $\gamma_1<0$. The range of these eigenvalues can be determined by relaxing any one of the boundary conditions (33), either $F_0(\eta)$ or $G_0(\eta)$ (Harris et al. 2009). Then, (30) and (31) are solved subject to the following boundary conditions:

$$F_0(0) = 0,\ F_0'(0) = 0,\ G_0' = \phi G_0(0),\ F_0''(0) = 1, \quad (34)$$

$$G_0(\infty) \to 0. \quad (35)$$

The unknown eigenvalues are computed using the *bvp4c* solver in MATLAB.

## NUMERICAL PROCEDURE

MATLAB's built-in function called the *bvp4c* is a finite difference code that implements a collocation method for the solution of boundary value problem (Rosca et al. 2012). In the present study, the *bvp4c* is used to compute the numerical solution of the boundary value problem (9)-(12). The usage of the *bvp4c* requires the differential (9) and (10) to be rewritten as a system of first order differential equations by using the following substitutions:

$$f = y(1),$$

$$f' = y(1)' = y(2),$$

$$f'' = y(2)' = y(3),$$

$$f''' = y(3)' = \frac{\left[-y(1)y(3) + \left(\frac{2m}{m+1}\right)(y(2))^2 + M^2 y(2)\right]}{[1 + nWe^2(y(3))^2][1 + We^2(y(3))^2]^{\frac{n-3}{2}}}. \quad (36)$$

$$\theta = y(4),$$

$$\theta' = y(4)' = y(5),$$

$$\theta'' = y(5)' = -Pry(1)y(5) + \frac{4}{3N_R}\frac{d}{d\eta}$$
$$[(1 + (\theta_w - 1)y(4))^3 y(5)]. \quad (37)$$

Then, the boundary conditions (11) and (12) become:

$$ya(1) = s,\ ya(2) = \lambda,\ ya(5) = -\phi[1 - ya(4)], \quad (38)$$

$$yb(2) \to 0,\ \ yb(4) \to 0. \quad (39)$$

The *bvp4c* solver has the syntax of `sol = bvp4c (odefun,bcfun,solinit,options)` (Shampine et al. 2003). Equations (36) and (37) are coded into the function handle `odefun` while the boundary conditions (38) and (39) are coded into the function handle `bcfun`. Whereas, the function handle `solinit` contains the initial guess of the solution and `options` defines the integration setting. Multiple solutions are obtained when different initial guesses made in `solinit` result in different solutions that satisfy the boundary conditions (38) and (39).

The method used is validated by comparing the present results with the published results of Khan et al. (2016), as shown in Table 1. The previous results by Khan et al. (2016) were computed using the Runge-Kutta Fehlberg integration scheme. Based on Table 1, the results are found to be in good agreement. Thus, verifying the method used in the present study.

For stability analysis, the same procedure is done by using the following substitutions:

$$F_0 = y(1), \qquad f_0 = s(1),$$

$$F_0' = y(2), \qquad f_0' = s(2),$$

$$F_0'' = y(3), \qquad f_0'' = s(3),$$

$$G_0 = y(4) \qquad \theta_0 = s(4),$$

$$G_0' = y(5), \qquad \theta_0' = s(5).$$

## RESULTS AND DISCUSSION

The variation of skin friction coeffcient, $Re^{1/2}C_{fx}$ and Nusselt number, $Re^{-1/2}Nu_x$ with the shrinking parameter, $\lambda$ for various values of the suction parameter, $s$, and radiation parameter, $N_R$ are presented in Figures 2 to 4. In these figures, $\lambda_c$ is the critical point at which the solution is unique. Dual solutions are obtained when the value of $\lambda > \lambda_c$, while no solution when $\lambda < \lambda_c$. In Figure 2, the skin friction coeffcient of the first solution increases with $s$. The imposition of suction moves the fluid closer to the sheet surface. The fluid movement then becomes inhibited by the sheet and causes the shear stress and the skin friction on the sheet surface to increase (Soid et al. 2018). However, the opposite occurs for the second solution. Besides that, suction will also increase the surface heat flux and improves the rate of heat transfer. In consequence, increases the Nusselt number, as observed in Figure 3. Meanwhile, the values of $Re^{1/2}C_{fx}$ and $Re^{-1/2}Nu_x$ of the first solution increase with $M$, as obtained in Table

TABLE 1. Values of $Re^{1/2}Cf_x$ and $Re^{-1/2}/Nu_x$ when $s = 0, \lambda = 1, Pr = 1.5, N_R = 1.0, \theta_w = 1.5, n = 0.5$ and $\phi = 0.3$

| $M$ | $We$ | $m$ | $Re^{1/2}Cf_x$ | | $Re^{-1/2}/Nu_x$ | |
|---|---|---|---|---|---|---|
| | | | Present study | Khan et al. (2016) | Present study | Khan et al. (2016) |
| 0.0 | 2.0 | 1.5 | -0.976814901 | -0.976815 | 0.585080891 | 0.585077 |
| 0.5 | - | - | -1.057524649 | -1.057526 | 0.565702201 | 0.565682 |
| 1.0 | - | - | -1.248575673 | -1.248588 | 0.513372562 | 0.513053 |

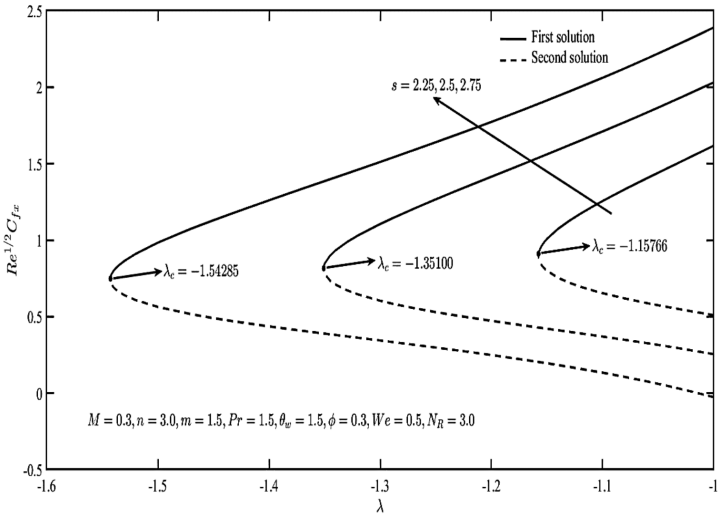


FIGURE 2. Variation of $Re^{1/2}Cf_x$ with $\lambda$ and $s$

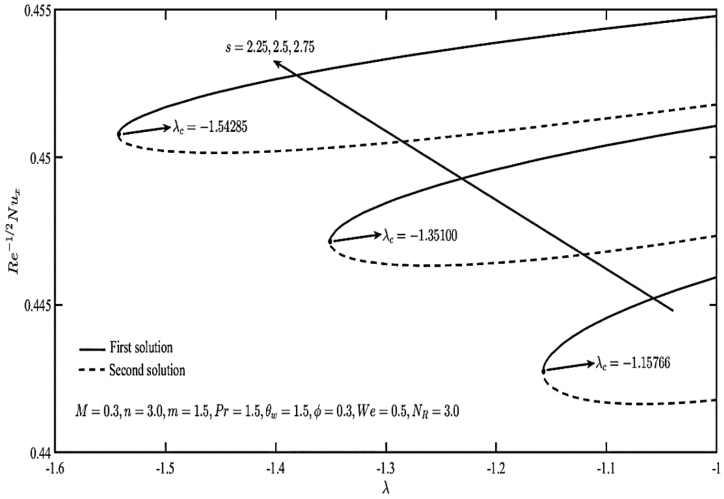


FIGURE 3. Variation of $Re^{-1/2}Nu_x$ with $\lambda$ and $s$

TABLE 2. Values of $Re^{1/2}Cf_x$ and $Re^{-1/2}/Nu_x$ for various $M$, $s$ and $\lambda$ when $\mathrm{Pr} = 1.5, N_R = 3.0, \theta_w = 1.5, \phi = 0.3, n = 3.0$ and $m = 1.5$

| *We* | *M* | *s* | $\lambda$ | $Re^{1/2}Cf_x$ | | $Re^{-1/2}/Nu_x$ | |
|---|---|---|---|---|---|---|---|
| | | | | First solution | Second solution | First solution | Second solution |
| 0.5 | 0.1 | 2.50 | -1.0 | 1.954221359 | 0.341970520 | 0.451016040 | 0.447932144 |
| | - | - | -1.1 | 1.626426225 | 0.454715009 | 0.450319382 | 0.447448574 |
| | - | - | -1.2 | 1.311896578 | 0.570300324 | 0.449431260 | 0.447150197 |
| | 0.2 | 2.50 | -1.0 | 1.983935823 | 0.308637357 | 0.451036855 | 0.447728588 |
| | - | - | -1.1 | 1.659169801 | 0.421623367 | 0.450352597 | 0.447222869 |
| | - | - | -1.2 | 1.353190638 | 0.530953764 | 0.449495914 | 0.446887077 |
| | 0.3 | 2.50 | -1.0 | 2.031502671 | 0.254900198 | 0.451069261 | 0.447339065 |
| | - | - | -1.1 | 1.710625207 | 0.369349616 | 0.450402871 | 0.446800721 |
| | - | - | -1.2 | 1.414859780 | 0.472273869 | 0.449586914 | 0.446417545 |
| 0.7 | 0.3 | 2.50 | -1.0 | 1.917180334 | 0.271887470 | 0.450770076 | 0.447385721 |
| | - | - | -1.1 | 1.570297391 | 0.397449508 | 0.449987918 | 0.446891364 |
| | - | - | -1.2 | 1.226708267 | 0.533776363 | 0.448951584 | 0.446651265 |

2. The increase in magnetic parameter causes the velocity gradient, ($f''(0)$) and temperature gradient, ($\theta'(0)$) to increase, which agrees with the results obtained by Soid et al. (2018). However, the opposite result is obtained for the second solution. In contrast, the increase in *We* reduces the values of $Re^{1/2}C_{fx}$ and $Re^{-1/2}Nu_x$ of the first solution, and conversely for the second solution. In Figure 4, the increase in $N_R$ is noted to reduce the Nusselt number. Hence, implying the reduction of heat transfer rate by the radiation parameter.

Next, the velocity and temperature profiles for various values of $s$ and $\lambda$ are shown in Figures 5 to 9. The validity of the numerical results is supported when the profiles reach the free stream boundary conditions (12) asymptotically. In Figure 5, the velocity profile of the first solution increases as increases, while the opposite occurs for the second solution. The imposition of suction brings the fluid closer to the sheet and reduces the boundary layer thickness. Hence, the velocity gradient increases, and the skin friction coeffcient and fluid velocity increase; this explains the results of the first solution. However, the increase in the magnitude of $\lambda$ is observed to reduce the velocity profile of the first solution, as seen in Figure 6. According to Yahaya Shagaiya et al. (2018), this is because the fluid flow is against the direction of the shrinking sheet. The boundary layer thickness of the first solution becomes greater as $|\lambda|$ increases. In Figure 7, the increase in $s$ reduces the temperature profiles of both solutions. The thermal boundary layer thickness becomes smaller as suction increases; this causes the temperature gradient and Nusselt number to increase, as obtained in Figure 3. Meanwhile, the temperature profiles of both solutions increase with the increasing magnitude of $\lambda$, as shown in Figure 8. Contrary, the increase in $N_R$ reduces the temperature profiles of both solutions in Figure 9. The mean absorption coeffcient increases as $N_R$ increases, which causes the radiative heat flux in (6) to decrease; this reduces the fluid temperature.

Then, a stability analysis is done to determine the stability and significance of the dual solutions. The

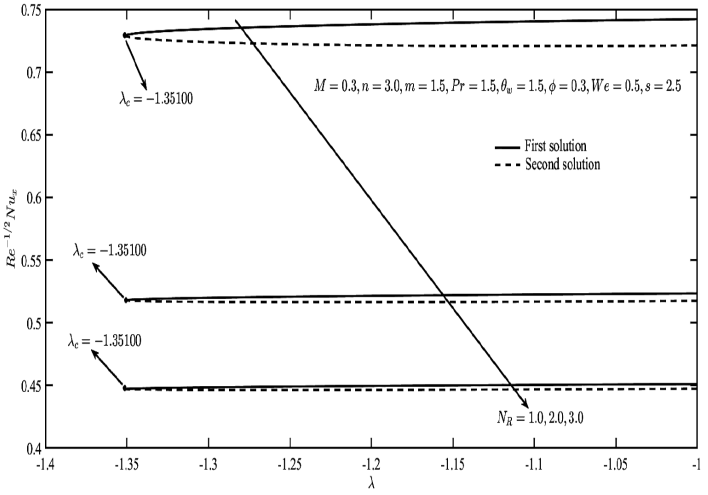


FIGURE 4. Variation of $Re^{-1/2}Nu_x$ with $\lambda$ and $N_R$

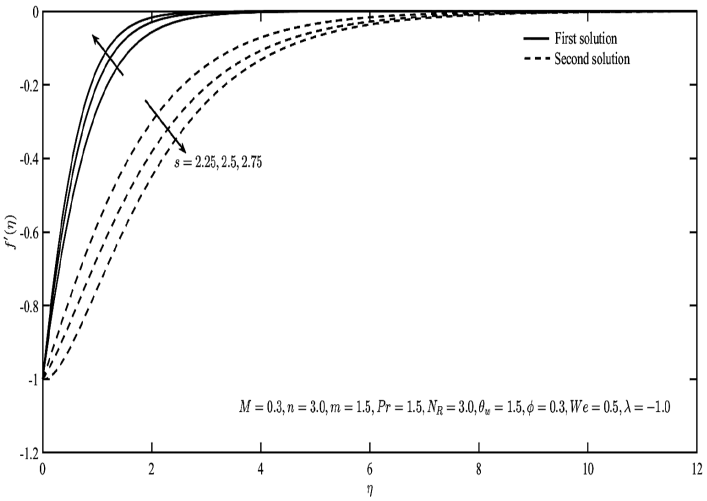


FIGURE 5. Velocity profile for various values of $s$

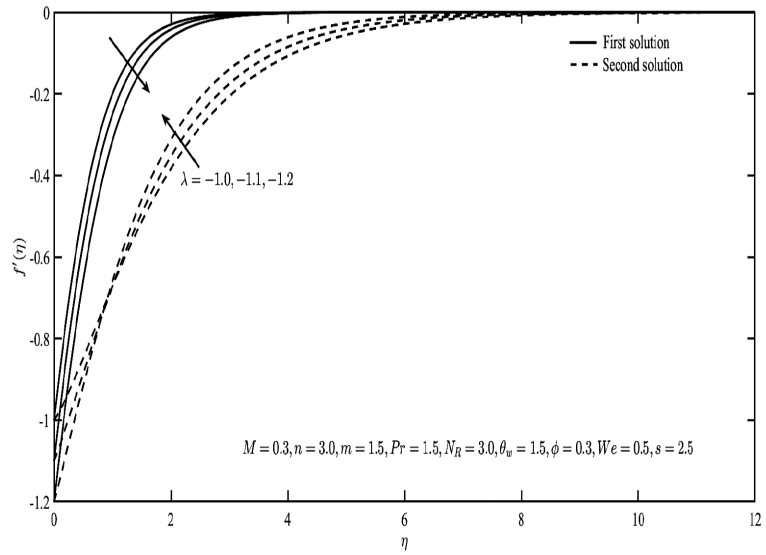


FIGURE 6. Velocity profile for various values of $\lambda$

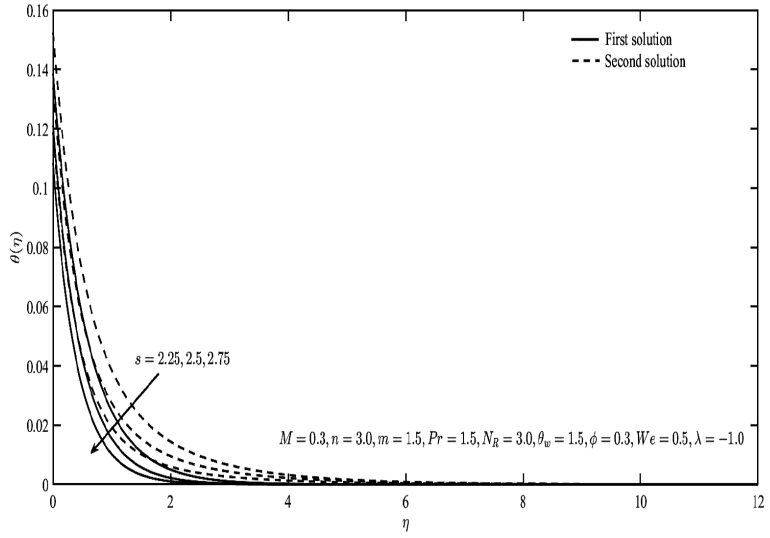


FIGURE 7. Temperature profile for various values of $s$

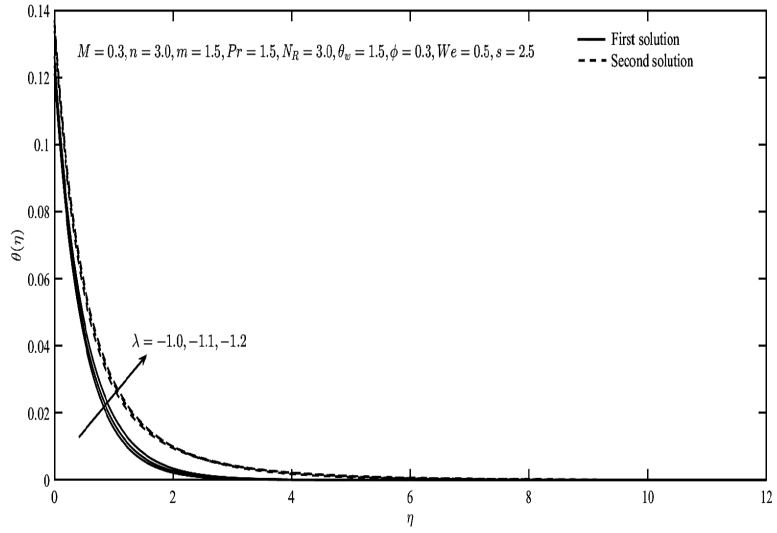


FIGURE 8. Temperature profile for various values of $\lambda$

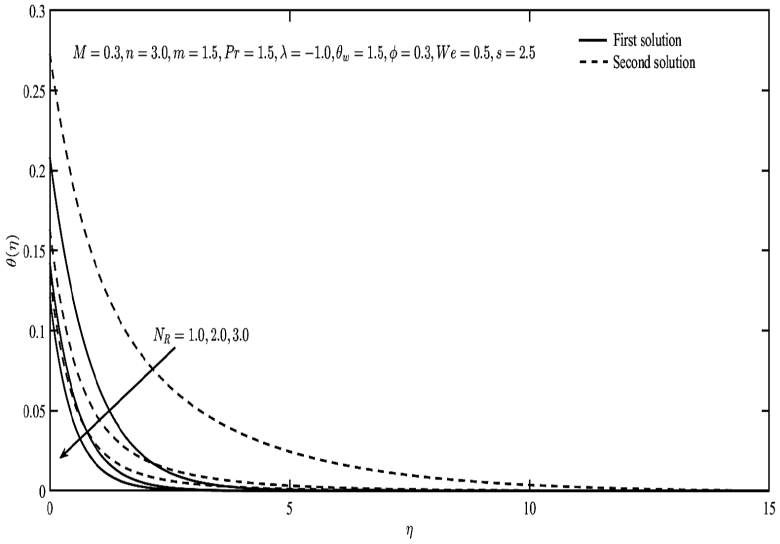


FIGURE 9. Temperature profile for various values of $N_R$

TABLE 3. Smallest eigenvalues, $\gamma_1$ for various values of $s$ and $\lambda$ when $M = 0.3$, $n = 3.0$, $m = 1.5$, $Pr = 1.5$, $N_R = 3.0$, $\theta_w = 1.5$, $\phi = 0.3$ and $We = 0.5$

| $s$ | $\lambda$ | $\gamma_1$ | |
|---|---|---|---|
| | | First solution | Second solution |
| 2.25 | –1.1 | 0.48120 | –0.45695 |
| | –1.15 | 0.16990 | –0.18244 |
| | –1.1576 | 0.00126 | –0.01942 |
| 2.50 | –1.3 | 0.51323 | –0.49069 |
| | –1.35 | 0.06529 | –0.07812 |
| | –1.3508 | 0.02428 | –0.03768 |
| 2.75 | –1.5 | 0.91437 | –0.50152 |
| | –1.54 | 0.13921 | –0.13266 |
| | –1.5428 | 0.01726 | –0.01254 |

smallest eigenvalues for the first and second solutions are computed using the *bvp4c* solver, and the results are tabulated in Table 3. Based on the table, the first solution has positive values of $\gamma_1$, while the second solution has negative values of $\gamma_1$. According to Awaludin et al. (2016), the positive value of $\gamma_1$ indicates a stable flow, while the negative value of $\gamma_1$ indicates an unstable flow. Therefore, the stable solution in this problem is the first solution, whereas the second solution is not stable. The first solution is realizable in practice and physically meaningful; thus, significant to this problem.

## CONCLUSION

Stability analysis is done to the dual solutions obtained in the problem of MHD Carreau fluid flow over a permeable shrinking sheet with thermal radiation. For the stability analysis, the problem is considered to be unsteady. The governing partial differential equations are transformed into ordinary differential equations using the similarity transformations. Then, time-dependent solutions are substituted into the equations to form linear eigenvalue equations. These equations are solved, for the smallest eigenvalues, by using the *bvp4c* solver in MATLAB. The results showed that the first solution has a positive smallest eigenvalue, while the second solution has a negative smallest eigenvalue. Thus, the first solution is stable and significant to the problem.

## ACKNOWLEDGEMENTS

The authors would like to thank Universiti Putra Malaysia for the financial support, received in the form of Putra Grant [9570600]. Authors contributions is as follows: Conceptualization of problem, R.I.Y. and N.M.A. Formal analysis of the problem and solution, R.I.Y. Validation, R.I.Y., N.M.A. and S.S.P.M.I. Original draft preparation, R.I.Y. Review and editing, R.I.Y., N.M.A. and S.S.P.M.I. Supervision, N.M.A. and S.S.P.M.I.

REFERENCES


Akbar, N.S., Nadeem, S., Haq, R.U. & Ye, S. 2014. MHD stagnation point flow of Carreau fluid toward a permeable shrinking sheet: Dual solutions. *Ain Shams Eng. J.* 5: 1233-1239.

Alamri, S.Z., Khan, A.A., Azeez, M. & Ellahi, R. 2019. Effects of mass transfer on MHD second grade fluid towards stretching cylinder: A novel perspective of Cattaneo-Christov heat flux model. *Phys. Lett. A*. 383(2-3): 276-281.

Arifin, N.M., Yusof, S.N. & Ismail, N.S. 2017. Slip effects on MHD stagnation-point flow of carreau fluid past a permeable shrinking sheet. *Matter: Int. J. Sci. Technol.* 3: 525-532.

Awaludin, I.S., Weidman, P.D. & Ishak, A. 2016. Stability analysis of stagnation-point flow over a stretching/shrinking sheet. *AIP Adv*. 6: 045308.

Bhatti, M.M., Zeeshan, A., Ellahi, R. & Shit, G.C. 2018. Mathematical modeling of heat and mass transfer effects on MHD peristaltic propulsion of two-phase flow through a Darcy-Brinkman-Forchheimer porous medium. *Adv. Powder Technol.* 29(5): 1189-1197.

Bhatti, M.M., Shahid, A. & Rashidi, M.M. 2016. Numerical simulation of fluid flow over a shrinking porous sheet by successive linearization method. *Alexandria Eng. J.* 55(1): 51-56.

Harris, S.D., Ingham, D.B. & Pop, I. 2009. Mixed convection boundary-layer flow near the stagnation point on a vertical surface in a porous medium: Brinkman model with slip. *Transport Porous Med.* 77: 267-285.

Hashim & Khan, M. 2017. Critical values in flow patterns of Magneto-Carreau fluid over a circular cylinder with diffusion species: Multiple solutions. *J. Taiwan Inst. Chem. E.* 77: 282292.

Hashim, Khan, M., Alshomrani, A.S. & Haq, R.U. 2018a. Investigation of dual solutions in flow of a non-Newtonian fluid with homogeneous-heterogeneous reactions: Critical points. *Eur. J. Mech. B/Fluids***.** 68: 30-38.

Hashim, Khan, M., Sharjeel & Khan, U. 2018b. Stability analysis in the transient flow of Carreau fluid with non-linear radiative heat transfer and nanomaterials: Critical points. *J. Mol. Liq.* 272: 787-800.

Hashim, Khan, M. & Alshomrani, A.S. 2017. Numerical simulation for flow and heat transfer to Carreau fluid with magnetic field effect: Dual nature study. *J. Magn. Magn. Mater.* 443: 13-21.

Irgens, F. 2014. *Rheology and Non-Newtonian* fluids. New York: Springer International Publishing.

Kamal, F., Zaimi, K., Ishak, A. & Pop, I. 2019. Stability analysis of MHD stagnation-point flow towards a permeable stretching/shrinking sheet in a nanofluid with chemical reactions effect. *Sains Malaysiana* 48(1): 243-250.

Khan, M., Sardar, H., Gulzar, M.M. & Alshomrani, A.S. 2018. On multiple solutions of non-Newtonian Carreau fluid flow over an inclined shrinking sheet. *Results Phys.* 8: 926-932.

Khan, M., Hussain, M. & Azam, M. 2016. Magnetohydrodynamic flow of Carreau fluid over a convectively heated surface in the presence of non-linear radiation. *J. Magn. Magn. Mater.* 412: 63-68.

Lok, Y.Y., Ishak, A. & Pop, I. 2011. MHD stagnation point flow with suction towards a shrinking sheet. *Sains Malaysiana* 40(10): 1179-1186.

Mahapatra, T.R. & Nandy, S.K. 2011. Stability analysis of dual solutions in stagnation-point flow and heat transfer over a power-law shrinking surface. *Int. J. Nonlinear Sci.* 12(1): 86-94.

Merkin, J.H. 1986. On dual solutions occurring in mixed convection in a porous medium. *J. Eng. Math.* 20: 171-179.

Miklavčič, M. & Wang, C. 2006. Viscous flow due to a shrinking sheet. *Q. Appl. Math.* 64(2): 283-290.

Naganthran, K. & Nazar, R. 2016. Stability analysis of MHD stagnation-point flow towards a permeable stretching/shrinking surface in a Carreau fluid. *AIP Conf. Proc.* 1750(1): 030031.

Rosca, N.C., Grosan, T. & Pop, I. 2012. Stagnation-point flow and mass transfer with chemical reaction past a permeable stretching/shrinking sheet in a nanofluid. *Sains Malaysiana* 41(10): 1271-1279.

Santhosh, H.B., Mahesha, Raju, S.S.K. & Raju, C.S.K. 2019. Comparative study on MHD carreau fluid due to stretching/shrinking surface in suspension of dust and graphene nanoparticles. *BioNanoSci.* 9(2): 483-494.

Santhosh, H.B., Mahesha & Raju, C.S.K. 2018. Carreau fluid over a radiated shrinking sheet in a suspension of dust and Titanium alloy nanoparticles with heat source. *J. Integr. Neurosci*. 17(3-4): 479-492.

Sarpkaya, T. 1961. Flow of non-Newtonian fluids in a magnetic field. *AIChE J*. 7(2): 324-328.

Shampine, L., Gladwell, I. & Thompson, S. 2003. *Solving ODEs with MATLAB*. Cambridge: Cambridge University Press.

Sheikholeslami, M., Ellahi, R., Shafee, A. & Li, Z. 2019. Numerical investigation for second law analysis of ferrofluid inside a porous semi annulus: An application of entropy generation and exergy loss. *Int. J. Numer. Method H*. 29(3): 1079-1102.

Sohail, A., Fatima, M., Ellahi, R. & Akram, K.B. 2019. A videographic assessment of ferrofluid during magnetic drug targeting: An application of artificial intelligence in nanomedicine. *J. Mol. Liq*. 285: 47-57.

Soid, S.K., Ishak, A. & Pop, I. 2018. MHD flow and heat transfer over a radially stretching/shrinking disk. *Chin. J. Phys*. 56: 58-66.

Soid, S.K., Ishak, A. & Pop, I. 2018. MHD stagnation-point flow over a stretching/shrinking sheet in a micropolar fluid with a slip boundary. *Sains Malaysiana* 47(11): 2907-2916.

Suneetha, S. & Gangadhar, K. 2015. Thermal radiation effect on MHD stagnation point flow of a Carreau fluid with convective boundary condition. *Open Sci. J. Math. Appl*. 3: 121.

Weidman, P.D., Kubitschek, D.G. & Davis, A.M.J. 2006. The effect of transpiration on self-similar boundary layer flow over moving surfaces. *Int. J. Eng. Sci*. 44: 730-737.

Yahaya Shagaiya Daniel, Zainal Abdul Aziz, Zuhaila Ismail & Faisal Salah. 2018. Effects of slip and convective conditions on MHD flow of nanofluid over a porous nonlinear stretching/shrinking sheet. *Aust. J. Mech. Eng*. 16: 213-229.



Rusya Iryanti Yahaya*, Norihan Md Arifin & Siti Suzilliana Putri Mohamed Isa
Institute for Mathematical Research
Universiti Putra Malaysia
43400 UPM Serdang, Selangor Darul Ehsan
Malaysia

Norihan Md Arifin
Department of Mathematics
Universiti Putra Malaysia
43400 UPM Serdang, Selangor Darul Ehsan
Malaysia

Siti Suzilliana Putri Mohamed Isa
Centre of Foundation Studies for Agricultural Science
Universiti Putra Malaysia
43400 UPM Serdang, Selangor Darul Ehsan
Malaysia

*Corresponding author; email: rusyairyanti@gmail.com

Received: 3 April 2019
Accepted: 7 September 2019